Periodica Polytechnica Mechanical Engineering, 66(4), pp. 344–349, 2022

Microstructure and Corrosion Properties of Austenitic and Duplex Stainless Steel Dissimilar Joints

Balázs Varbai[1*], Patrik Bolyhos[1], Dávid Miklós Kemény[1], Kornél Májlinger[1]

[1] Department of Materials Science and Engineering, Faculty of Mechanical Engineering, Budapest University of Technology and Economics, Budapest, Műegyetem rakpart 3., 1111, Budapest, Hungary
[*] Corresponding author, e-mail: kemeny.david@gpk.bme.hu

Received: 17 August 2022, Accepted: 13 September 2022, Published online: 06 October 2022

Abstract

In several applications duplex stainless steels should be joint welded to conventional austenitic stainless steels. In this research LDX 2101 lean duplex stainless steel sheets were welded to conventional 304 austenitic stainless steels, using gas tungsten arc welding. For the welded joints three different welding rods were used: ER 308L, ER 309LSi, and ER 2209. For gas shielding two different shielding gases were used: argon and argon +2% nitrogen. It was found that the nitrogen addition to the shielding gas promoted austenite formation in the weld metal. It was also found Schaeffler-diagram modified by Outokumpu showed a very good estimation to the ferrite content and chemical composition of the weld metal. The ferrite content estimated by the Outokumpu-diagram, showed a close correlation to measured ferrite contents, the highest error was 30%. In case of the chemical composition of the weld metal, the Cr- and Ni-contents were estimated with a maximum of 15% error. In terms of the corrosion resistance, the best pitting corrosion resistance was achieved using the 308L welding rod with argon shielding gas, where the weight loss was 1.6% after the 24 hours immersion test.

Keywords

duplex stainless steel, dissimilar welded joints, corrosion, prediction of ferrite content, austenitic stainless steel

1 Introduction

Duplex stainless steels have great strength (yield strength, $R_{p0.2} \approx 500$ MPa) and excellent corrosion resistance especially against stress corrosion [1–5]. Thus, the application of duplex stainless steels (DSSs) in civil engineering, chemical, oil and gas industries are constantly growing [6–9]. Among duplex stainless steels the low nickel and molybdenum bearing lean duplex grades show the similar corrosion resistance as the conventional austenitic grades, however providing a much a higher strength and a lower price [10]. In several applications duplex and lean duplex stainless steels should be joint welded to conventional austenitic stainless steels with higher nickel and lower chromium contents [11, 12]. The different chemical composition results in different corrosion resistance and mechanical properties [13, 14]. Thus, potential problems can emerge from the inadequately selected welding consumable, welding process and preparation, which affects the dilution, and thus the abovementioned properties in the weld metal. From the operational weldability aspect, it is also significant, that the austenitic and duplex stainless steels have different physical properties, which can result in arc wandering or deformation dure to residual stresses.

The welding consumable selection determines the governing properties of the weld metals. Thus, designing the welded joints, joint preparations, dilution rate, etc. is essential in dissimilar joints between different stainless steels. For the design of dissimilar joints constitutional diagrams such as the Schaeffler-diagram can be used [15]. These diagrams show the governing microstructure in the weld metal according to the ferrite promoting elements (chromium equivalent, CrE) and the austenite promoting elements (nickel equivalent, NiE). Several constitutional diagrams exist, with different CrE and NiE calculation methods, however they do not calculate with the welding variables, such as the shielding gas, which can have a great influence on the microstructure. It is known that the nitrogen containing shielding gas in gas tungsten arc welding (GTAW) can promote austenite formation, thus small amount (2%) of nitrogen addition to the shielding gas is recommended [16].

In the current research, the dissimilar joints in-between LDX 2101 lean duplex and 304 austenitic stainless steels were investigated. The joints were welded by GTAW using

Cite this article as: Varbai, B., Bolyhos, P., Kemény, D. M., Májlinger, K. "Microstructure and Corrosion Properties of Austenitic and Duplex Stainless Steel Dissimilar Joints", Periodica Polytechnica Mechanical Engineering, 66(4), pp. 344–349, 2022. https://doi.org/10.3311/PPme.21007

3 different suitable welding rods and pure (4.6) argon and argon +2% nitrogen containing gas mixtures. The joints were evaluated by metallographic techniques and corrosion tests.

2 Materials and methods

2.1 Base materials and welding consumables

For the GTAW dissimilar joint experiments X2CrMnNi N21–5–1 (LDX 2101) lean duplex stainless steel sheet in 2 mm thickness with the size of 100 × 50 mm, and X5Cr Ni18–10 (AISI 304) austenitic stainless steel sheet in 3 mm thickness with the size of 100 × 40 mm were GTA welded together. The chemical compositions of the base materials can be seen in Table 1. and the mechanical properties in Table 2. For the dissimilar joints three different welding rods were used: W 19 9 L (ER 308L), W 23 12 L Si (ER 309LSi), and W 22 9 3 N L (E 2209). In the designation of the welding rods the numbers are referred to the weight percent of Cr, Ni and Mo, respectively. For GTAW of DSSs nitrogen containing gas mixtures are recommended [16, 17], thus argon and argon +2% nitrogen shielding gases were used.

Table 1 Chemical composition of the base materials, according to their data sheet

Base material	Chemical composition (weight %)						
	Cr	Ni	Mo	N	Cu	C	Mn
LDX 2101	21.5	1.5	0.3	0.22	0.3	0.03	5
AISI 304	18.3	8.6	0.2	-	0.4	0.005	1.8

Table 2 Mechanical properties of the base materials, according to their data sheet

Base material	Mechanical property (minimum)		
	$R_{p0.2}$ (MPa)	R_m (MPa)	A (%)
LDX 2101	530	700	30
AISI 304	230	540	45

Table 3 The welding parameters used for the dissimilar joint experiments

GTAW rod	Shielding gas	Welding Current (A)	Arc Voltage (V)	Travel speed (cm/min)	Arc energy (kJ/mm)
2209	Ar	57	12	7.1	0.58
308L	Ar	57	11.5	6.9	0.57
309LSi	Ar	57	12	7	0.59
2209	Ar+2N_2	57	13	7.2	0.62
308L	Ar+2N_2	57	13	7.1	0.60
309LSi	Ar+2N_2	57	13	7.3	0.61

2.2 Welding parameters

The applied welding parameters can be seen in Table 3. In Table 3 arc energy (thermal efficiency is considered as 1.0) is presented instead of heat input as different shielding gases were used with different physical properties. The arc energy was kept constant ~0.6 kJ/mm in every case. The shielding gas flow rate was 9 L/min, the argon backing gas flow rate was 5 L/min in every case. The length of the welds was 110 mm. The used polarity for the GTAW was DC−. The GTAW was done manually, thus the welding parameters presented in Table 3. are average values for each welding run. 2 mm root gap was kept, and no chamfering was used during welding in all cases.

2.3 Microstructure evaluation

The microstructural evaluation was done using standard metallographic specimens. The specimens were cut form the cross-section and mounted into metallographic resin. The mounted samples were grinded up to 4000 grit paper and then polished with 3 µm diamond suspension. To reveal the dissimilar microstructure two different types of etchants were used. For the lean duplex side Beraha-type etchant [18]: 60 ml H_2O + 20 ml HCl + 0.5 g $K_2S_2O_5$ was used for 5 s. For the austenitic side Kalling-type etchant [19]: 20 ml C_2H_5OH + 40 ml HCl + 2 g $CuCl_2$ was used for 25 s. For every etching sequence the Kalling-type etchant was used first. The ferrite content of the weld metal was measured using Fischer FMP30 ferritescope. The chemical composition of the weld metal was measured by scanning electron microscope (SEM) with energy dispersive spectroscopy (EDS), with Zeiss EVO MA10 SEM with EDAX EDS system. The dilution ratio was measured on the metallographic specimens, using Olympus SZX16 stereo microscope. The microstructural images were obtained by Olympus PMG3 optical microscope.

2.4 Prediction methods using constitutional diagrams

For the prediction of the weld metals chemical composition and ferrite content two different constitutional diagrams were used. The Schaeffler-diagram (S) [15] is the conventional constitutional diagram used for the prediction of stainless steel weld metals, which was a bit modified by the stainless steel manufacturer Outokumpu (O) [20]. The CrE and NiE values according to the constitutional diagrams (S and O) were calculated as in Eqs. (1)–(4):

$$\mathrm{CrE(S)} = \mathrm{Cr} + \mathrm{Mo} + 1.5 \times \mathrm{Si} + 0.5 \times \mathrm{Nb}\,, \tag{1}$$

$$\mathrm{NiE(S)} = \mathrm{Ni} + 30 \times \mathrm{C} + 0.5 \times \mathrm{Mn}\,, \tag{2}$$

$$\mathrm{CrE(O)} = \mathrm{Cr} + \mathrm{Mo} + 1.5 \times \mathrm{Si} + 0.5 \times \mathrm{Nb}\,, \quad (3)$$

$$\mathrm{NiE(O)} = \mathrm{Ni} + 30 \times (\mathrm{C} + \mathrm{N}) + 0.5 \times \mathrm{Mn}\,. \quad (4)$$

The chemical composition of the weld metal (X_{WM}) was predicted by the following Eq. (5):

$$X_{WM} = D_{2101} \times X_{2101} + D_{304} \times X_{304} + D_{cons} \times X_{cons}\,, \quad (5)$$

where D are the dilutions rate of the two base materials and the welding consumable, and X is the given alloying element in the base materials and the welding consumable.

2.5 Corrosion test

The welded sheets were first cut to 25 × 50 mm specimens, which were cleaned, pickled and passivated before the corrosion test, using Polinox P Rapid pickling paste for 15 minutes. The weights of the specimens were measured before and after 24 hours (according to ISO 17781 [21]) by Denver Instrument APX-200 with 0.1 mg accuracy. The corrosive media was 6% $FeCl_3$ aqueous solution according to ASTM G48 [22]. The type of the corrosion was also evaluated using stereo microscopic techniques.

3 Results and discussion

3.1 Weld metal microstructure

The weld metals microstructures can be seen in Fig. 1 on etched metallographic images. Using the ER 2209 DSS welding rod resulted in more ferritic microstructure (darker areas) with both shielding gases. Using the ER 308LSi austenitic stainless steel welding rod and the higher Cr- and Ni-containing 309LSi rod (recommended mostly for dissimilar welds) resulted in more austenitic microstructure. It can be also seen on the microstructure images, that the nitrogen addition to the shielding gas highly promoted austenite formation in the weld metal in all cases, but most significantly in the case of ER 308LSi welding rod. The heat affected zone (HAZ) showed mostly ferritic microstructure, which correlates to the results of Pandey et al. [23].

3.2 Evaluation according to the predictive diagrams

The dilution ratios were calculated on the cross-sections of the welded joints. One example for the calculation can be seen in Fig. 2, showing the ER 308LSi welded dissimilar joint, using Ar +2% N_2 shielding gas.

The dilution results can be seen in Table 4.

The welding consumable gave ~50–60% of the weld metal according to the measurements on the cross-sections. Some variations are measured, which is originated from the manual welding. Also, the shielding gas composition

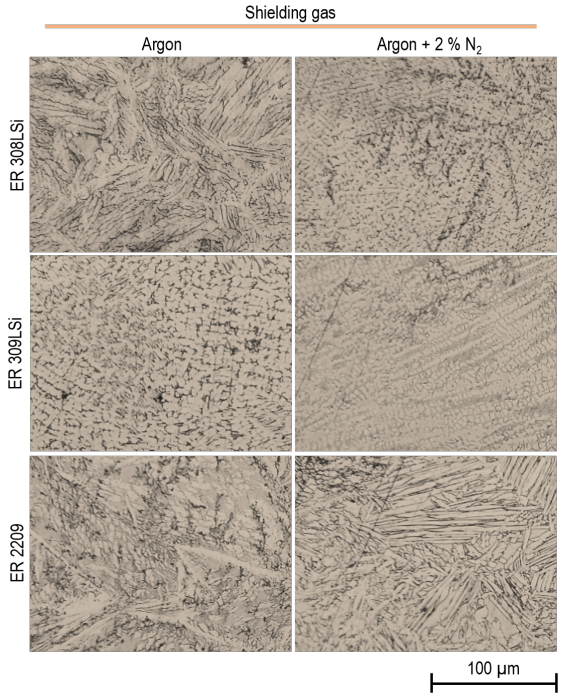

Fig. 1 The weld metal microstructures using different shielding gases and welding consumables. The darker area represents the ferrite the lighter area the austenite phase

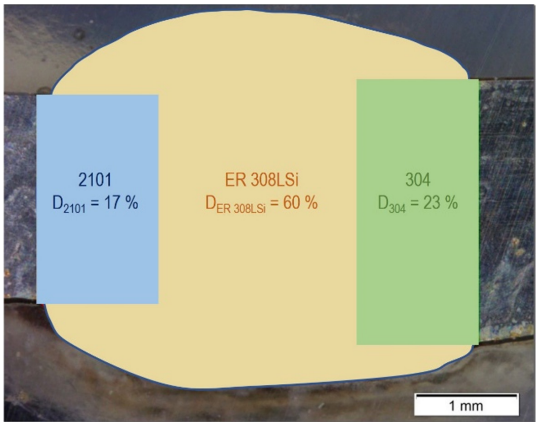

Fig. 2 Calculation of the dilution ratio according to the cross-sectional macroimage of the ER 308LSi, Ar +2% N_2 welded joint

Table 4 The different dilutions measured on the cross-sections of the welded joints

Shielding gas	Dilution (%)		
	D_{2101}	D_{304}	$D_{ER\ 308LSi}$
Ar	20	20	60
Ar + 2 % N_2	17	23	60
	D_{2101}	D_{304}	$D_{ER\ 308LSi}$
Ar	25	20	55
Ar + 2 % N_2	21	26	53
	D_{2101}	D_{304}	$D_{ER\ 308LSi}$
Ar	17	20	63
Ar + 2 % N_2	21	27	52

seems to influence the dilutions, as the properties of the arc plasma and thermal efficiency also differs. For the calculations of the chemical compositions and the ferrite contents the dilution rates were used in Eq. (5).

The comparison of the measured and estimated ferrite content of the weld metal can be seen in Table 5.

In Table 5. it is visible the nitrogen addition to the shielding gas has an austenite promoting effect. It is also confirmed that the most significant influence of nitrogen was measured in the weld made by ER 308LSi welding rod, which is also visible in Fig. 1. The ER 2209 welding rod resulted in a duplex weld metal, as the measured ferrite contents are ~ 30%. Comparing the constitutional diagrams, the Outokumpu-diagram is giving much closer estimation to the measured ferrite contents, because in the NiE(O) (Eq. (4)) nitrogen also presents as a strong austenite former. Also, the Outokumpu-diagram is modified to incorporate the modern nitrogen alloyed lean duplex stainless steel grades, by comparison to the original Schaeffler-diagram, which was first published in 1949.

The comparison of the measured and estimated chemical composition of the weld metal can be seen in Table 6. With SEM EDS the Cr, Ni, Mn, and Mo alloying content was measured, and were compared. For the comparison the Schaeffler-diagram was used.

From Table 6. it is visible the Schaeffler-diagram always underestimated the Cr-content and always overestimated the Mn-contents. The best estimation was in case of the ER 2209 welding rod. The shielding gas has an influence on the arc properties, thermal efficiency and thus the dilutions. The differences could be measured in the weld metal chemical compositions as a function of the shielding gas. The highest difference can be seen in the Mo- and Mn-contents, but the Cr- and Ni-contents show good correlation (highest error is 15% in case of ER 308 LSi with Ar shielding). It is not bad taking into attention that, the Schaeffler-diagram does not calculate with the welding variables.

3.3 Corrosion resistance

The surface of the face side of the argon shielding gas welded samples after the 24 hours of corrosion testing can be seen in Fig. 3, where the left side to the weld is always the LDX 2101 base material and the right side is the AISI 304.

In Fig. 3 it is visible pitting corrosion occurred after 24 hours on the austenitic steel side in all cases. This is due to the lower chromium of the austenitic grade compared to the 2101 lean duplex steel and also compared to the used three welding consumables. This type of corrosion

Table 5 The comparison of the measured and estimated ferrite contents of the weld metals

GTAW rod	Shielding gas	Ferrite (%)		
		Measured	Estimated S	Estimated O
ER 308LSi	Ar	15 ± 2	16	15
	Ar+2N_2	9 ± 3	15	13
ER 309LSi	Ar	12 ± 1	16	13
	Ar+2N_2	10 ± 3	14	12
ER 2209	Ar	31 ± 3	58	30
	Ar+2N_2	29 ± 5	50	27

Table 6 The comparison of the measured (EDS) and estimated (S – Schaeffler) chemical compositions of the weld metals welded with different GTAW rods and shielding gases

Elements (m%)	ER 308 LSi		ER 309 LSi		ER 2209	
	Ar	Ar+2%N_2	Ar	Ar+2%N_2	Ar	Ar+2%N_2
Cr (EDS)	22.7	29.2	24.7	21.8	24.0	21.9
Cr (S)	19.4	19.2	22.1	21.5	24.1	21.5
Ni (EDS)	6.7	9.4	8.9	7.3	7.1	7.8
Ni (S)	7.7	7.9	9.7	9.9	7.1	6.9
Mn (EDS)	1.5	1.6	1.3	1.1	0.7	1.1
Mn (S)	2.4	2.3	2.7	2.5	2.1	2.3
Mo (EDS)	0.7	0.3	0.6	0.5	2	1.6
Mo (S)	0.1	0.1	0.2	0.2	2.2	1.9

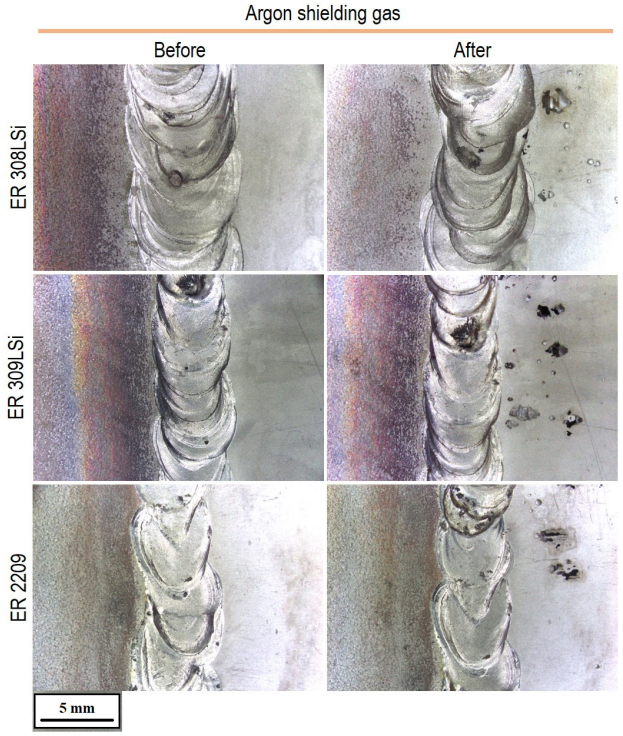

Fig. 3 The surface of the face side before and after the 24 h corrosion test of the argon welded samples. Left side of the weld: LDX 2101 base material, right side: AISI 304

mechanism is representative also to the samples welded with argon +2% nitrogen shielding gas. The weight loss of the specimens in percentages after the 24 h corrosion test can be seen in Fig. 4. The samples had fairly the same weight loss, the difference between the highest and lowest corrosion rate is only 1%. The reason for this is that the pitting corrosion initiated at the AISI 304 austenitic side in the base material, and the corrosion developed in these pitting sites. Thus, the welding consumable and the used shielding gas has a low influence on the corrosion resistance in this case. Also, the joints were welded with roughly the same arc energy, thus the heat cycle influence on the heat affected zone is also the same. Nevertheless, the lowest corrosion rate, 1.6% weight loss, was measured in case of ER 308LSi and ER 309LSi welding wires, which correlates to the results of Maurya et al. [24], who also found that ER 309LMo rod gave the best corrosion resistance for the dissimilar welding of superaustenitic and super duplex grades.

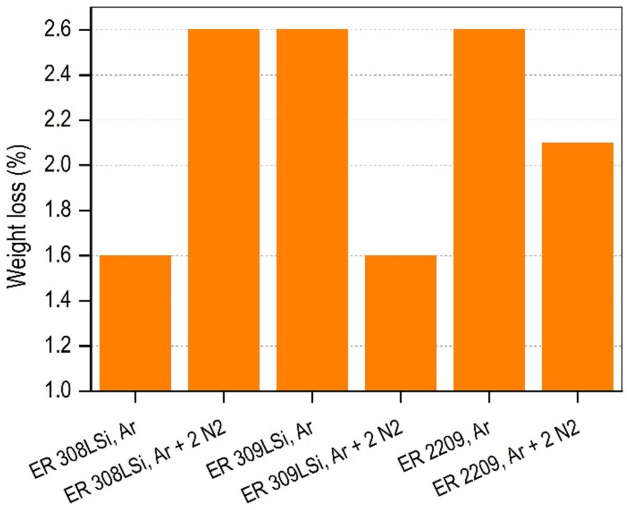

Fig. 4 The weight loss of the different welded specimens after the 24 h corrosion test

4 Conclusions

In our research we investigated dissimilar 2101 lean duplex (X2CrMnNiN21–5–1) – AISI 304 (X5CrNi18–10) austenitic stainless steel joints. The welds were made by gas tungsten arc welding, using three different welding rods: W 19 9 L (ER 308L), W 23 12 L Si (ER 309LSi), and W 22 9 3N L (ER 2209), and two different shielding gases: argon and argon +2% nitrogen.

It was found that both constitutional diagrams according to Schaeffler [15] and Outokumpu [20] can be used to predict the weld metal ferrite content and chemical composition with good correlation. The ferrite content could be estimated with a maximum error of 30% and the Cr- and Ni-contents in the weld metal were estimated with maximum 15% error.

It was also found the pitting corrosion initiated on the AISI 304 austenitic base material side in all cases during the 24 hours immersion test, thus the welding consumable and the shielding gas had no influence on the corrosion resistance of the welded joints. Nevertheless, the lowest corrosion resistance was measured in case of the ER 308LSi and ER 309LSi welding consumables, which was 1.6%.

Acknowledgement

This paper has been supported by the National Research, Development and Innovation Office – NKFIH, OTKA PD 138729.

This paper is recommended by the Hungarian Welding Society (MAHEG) and is the written extract of the conference presentation presented in the XXXI. International Welding Conference, Kecskemét, Hungary.

References

[1] de Farias Azevedo, C. R., Boschetti Pereira, H., Wolynec, S., Padilha, A. F. "An overview of the recurrent failures of duplex stainless steels", Engineering Failure Analysis, 97, pp. 161–188, 2019. https://doi.org/10.1016/j.engfailanal.2018.12.009

[2] Świerczyńska, A., Fydrych, D., Landowski, M., Rogalski, G., Łabanowski, J. "Hydrogen embrittlement of X2CrNiMoCuN25-6-3 super duplex stainless steel welded joints under cathodic protection", Construction and Building Materials, 238, 117697, 2020. https://doi.org/10.1016/j.conbuildmat.2019.117697

[3] Berecz, T., Fazakas, É., Fábián, E. R., Jenei, P., Maróti, J. E. "Investigation of Thermally Induced Deterioration Processes in Cold Worked SAF 2507 Type Duplex Stainless Steel by DTA", Crystals, 10(10), 937, 2020. http://doi.org/10.3390/cryst10100937

[4] Mészáros, I., Bögre, B., Szabó, P. J. "Magnetic and Thermoelectric Detection of Sigma Phase in 2507 Duplex Stainless Steel", Crystals, 12(4), 527, 2022. https://doi.org/10.3390/cryst12040527

[5] Mohan, D. G., Tomków, J., Karganroudi, S. S. "Laser Welding of UNS S33207 Hyper-Duplex Stainless Steel to 6061 Aluminum Alloy Using High Entropy Alloy as a Filler Material", Applied Sciences, 12(6), 2849, 2022. https://doi.org/10.3390/app12062849

[6] Nagy, A. I., Fábián, E. R., Horváth, R., Terek, P. "Difficulties in the Machining Super Duplex Stainless Steels", Műszaki Tudományos Közlemények, 11(1), pp. 141–144, 2019. https://doi.org/10.33894/mtk-2019.11.31

[7] Olsson, J., Snis, M. "Duplex - A new generation of stainless steels for desalination plants", Desalination, 205(1–3), pp. 104–113, 2007. https://doi.org/10.1016/j.desal.2006.02.051

[8] Boillot, P., Peultier, J. "Use of stainless steels in the industry: recent and future developments", Procedia Engineering, 83, pp. 309–321, 2014. https://doi.org/10.1016/j.proeng.2014.09.015

[9] Payares-Asprino, C. "Prediction of Mechanical Properties as a Function of Welding Variables in Robotic Gas Metal Arc Welding of Duplex Stainless Steels SAF 2205 Welds Through Artificial Neural Networks", Advances in Materials Science, 21(3), pp. 75–90, 2021. https://doi.org/10.2478/adms-2021-0019

[10] Rogalski, G., Świerczyńska, A., Fydrych, D., Landowski, M. "The influence of solution annealing temperature on the properties of Lean Duplex 2101 welded joints in tubes", Welding Technology Review, 91(4), pp. 49–59, 2019. https://doi.org/10.26628/wtr.v91i4.1017

[11] Landowski, M., Świerczyńska, A., Rogalski, G., Fydrych, D. "Autogenous Fiber Laser Welding of 316L Austenitic and 2304 Lean Duplex Stainless Steels", Materials, 13(13), 2930, 2020. https://doi.org/10.3390/ma13132930

[12] Dobránszky, J., Lőrinc, Z., Gyímesi, F., Szigethy, A., Bitay, E. "Laser welding of lean duplex stainless steels and their dissimilar joints", presented at 8th European Stainless Steel and Duplex Stainless Steel Conference, Graz, Austria, April, 28–30, 2015.

[13] Kemény, D. M., Kovács, D. "The Effect of Welding Parameters on the Corrosion Resistance of Austenitic Stainless Steel", Periodica Polytechnica Mechanical Engineering, 66(2), pp. 151–157, 2022. https://doi.org/10.3311/PPme.19568

[14] Kovács, D., Dobránszky, J. "Effects of Thermochemical Surface Treatments on the Industrially Important Properties of X2CrNiMo 17-12-2 Austenitic Stainless Steel", Periodica Polytechnica Mechanical Engineering, 63(3), pp. 214–219, 2019. https://doi.org/10.3311/PPme.13921

[15] Schaeffler, A. L. "Constitutional Diagram for Stainless Steel Weld Metal", Metal Progress, 56, pp. 680–680B, 1949.

[16] Hertzman, S. "The influence of nitrogen on microstructure and properties of highly alloyed stainless steel welds", ISIJ International, 41(6), pp. 580–589, 2001. https://doi.org/10.2355/isijinternational.41.580

[17] Varbai, B., Adonyi, U. Y., Baumer, R., Pickle, T., Dobránszky, J., Májlinger, K. "Weldability of Duplex Stainless Steels-Thermal Cycle and Nitrogen Effects", Welding Journal, 98(3), pp. 78-S–87-S, 2019. https://doi.org/10.29391/2019.98.006

[18] Varbai, B., Májlinger, K. "Optimal etching sequence for austenite to ferrite ratio evaluation of two lean duplex stainless steel weldments", Measurement, 147, 106832, 2019. https://doi.org/10.1016/j.measurement.2019.07.060

[19] Ozlati, A., Movahedi, M. "Effect of welding heat-input on tensile strength and fracture location in upset resistance weld of martensitic stainless steel to duplex stainless steel rods", Journal of Manufacturing Processes, 35, pp. 517–525, 2018. https://doi.org/10.1016/j.jmapro.2018.08.039

[20] Outokumpu "Handbook of Stainless Steel", [online] Available at: https://www.outokumpu.com/en/expertise/2021/handbook-of-stainless-steel [Accessed: 18 July 2022]

[21] ISO "ISO 17781:2017 Petroleum, petrochemical and natural gas industries — Test methods for quality control of microstructure of ferritic/austenitic (duplex) stainless steels", International Organization for Standardization, Geneva, Switzerland, 2017.

[22] ASTM "ASTM G48-11(2015) Standard Test Methods for Pitting and Crevice Corrosion Resistance of Stainless Steels and Related Alloys by Use of Ferric Chloride Solution", ASTM International, West Conshohocken, PA, USA, 2015. https://doi.org/10.1520/G0048-11R15

[23] Pandey, C., Thakare, J. G., Taraphdar, P. K., Kumar, P., Gupta, A., Sirohi, S. "Characterization of the soft zone in dissimilar welds joint of 2.25Cr-1Mo and lean duplex LDX2101 steel", Fusion Engineering and Design, 163, 112147, 2021. https://doi.org/10.1016/j.fusengdes.2020.112147

[24] Maurya, A. K., Pandey, C., Chhibber, R. "Dissimilar welding of duplex stainless steel with Ni alloys: A review", International Journal of Pressure Vessels and Piping, 192, 104439, 2021 https://doi.org/10.1016/j.ijpvp.2021.104439